1.E.7:2.G *Nuclear Physics* A271 (1976) 77—94;

ISOBARIC ANALOG STATES OF THE TIN AND TELLURIUM ISOTOPES STUDIED WITH THE (^{3}He, t) REACTION AT $\theta_L = 0°$

F. D. BECCHETTI, W. S. GRAY, J. JÄNECKE, E. R. SUGARBAKER and R. S. TICKLE
Physics Department, The University of Michigan Ann Arbor, Michigan 48109, USA†

Received 2 April 1976
(Revised 22 June 1976)

Abstract: The Sn(^{3}He, t)Sb and Te(^{3}He, t)I reactions to the g.s. isobaric analog states (IAS) of ^{112,114,116,117,118,119,120,122,124}Sn and ^{124,125,126,128,130}Te have been studied at $\theta = 0°$ and $E(^3\text{He}) = 45.9$ MeV. The Coulomb displacement energies decrease more slowly than $A^{-\frac{1}{3}}$ indicating that the rms radius of the nuclear matter distribution increases more slowly than $A^{\frac{1}{3}}$. The total widths of the IAS are 10 to 60 keV and exhibit a pronounced odd-A even-A variation correlated with the excitation and decay energies of the IAS. Estimates of the decay and spreading widths have been obtained, with the latter yielding an isospin-mixing matrix element of about 1 keV. The (^{3}He, t) cross sections at 0° appear to be directly related to (p, n) total cross sections for the 0^+ IAS. The cross sections for the Sn-Sb and Te-I isotopes, in contrast to accepted expressions, depend in a complicated manner on the neutron excess. A microscopic analysis gives an effective interaction ($\mu = 1$ fm^{-1}) of $V_{t\cdot t} = 11 \pm 4$ MeV. This is smaller than values obtained from analyses of (^{3}He, t) reactions on nuclei with $A \lesssim 90$, if one assumes a simple direct charge-exchange reaction.

E NUCLEAR REACTIONS ^{112,114,116,117,118,119,120,122,124}Sn, ^{124,125,126,128,130}Te(^{3}He, t), $E = 45.9$ MeV; measured $\sigma(E_t, \theta = 0°)$. ^{112,114,116,117,118,119,120,122,124}Sb, ^{124,125,126,128,130}I deduced IAS, Coulomb displacement energies, Γ. Enriched targets, magnetic spectrometer.

1. Introduction

While much is known about isobaric analog states (IAS) of the odd-A isotopes in the Sn-Te region, data for the even-A nuclei are sparse. This is because in proton resonance experiments [1-3]), hitherto the main source of data on IAS in this mass region, mainly analogs of odd-A systems (proton plus even-A target) have been studied.

We have used the (^{3}He, t) reaction on the targets ^{112,114,116,117,118,119,120,122,124}Sn and ^{124,125,126,128,130}Te to obtain information on the IAS of even-A as well as some odd-A Sn and Te isotopes. The (^{3}He, t) reaction (particularly at $\theta_L = 0°$) has several advantages over the alternate (p, n) reaction for the study of IAS. The energy resolution of $\lesssim 20$ keV is usually much better, permitting accurate determination of Coulomb energies and IAS widths. Furthermore, at forward angles the background from compound nucleus decay is much smaller relative to the IAS

† Work supported in part by USERDA Contract E-(11-1)-2167.

allowing accurate measurements of the IAS centroid and cross section. Information on the even-A isotopes is particularly valuable since these nuclei are stable and have been studied extensively by other means. Thus empirical charge distributions and nuclear wave functions are often available.

2. Experiment

The measurements were made with a 45.9 MeV $^3He^{++}$ beam from The University of Michigan 83 inch cyclotron. Tritons from the (^{3}He, t) reaction were detected at $\theta_L = 0°$ using the arrangement shown in fig. 1. The incident beam after passing through the target was bent and stopped in an aluminum baffle placed in the first analyzing magnet. The tritons, which are much more rigid magnetically, were detected in the focal plane of either the first (AM1) or second (AM2) analyzing magnet.

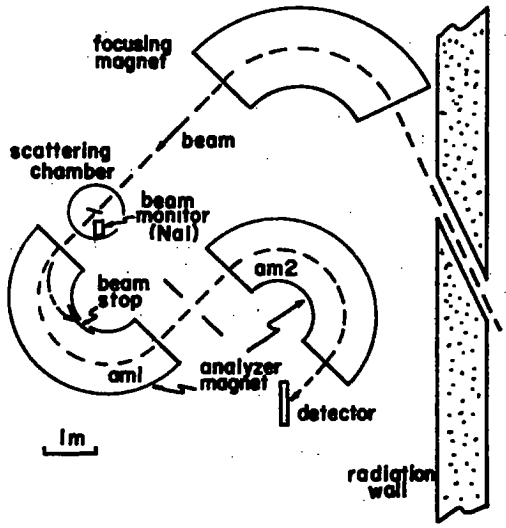

Fig. 1. Experimental set-up for 0° measurements.

The latter permitted measurements with large dispersion (6 keV/mm) and complete dispersion matching so as to cancel beam energy spread. Most of the data were obtained with a single calibrated solid-state position-sensitive detector (PSD) with an active length of 5 cm. Particle identification was made utilizing the PSD energy signal and a position signal obtained by analog division of the XE and E signals. A few spectra were also obtained with a 25 cm long position-sensitive proportional counter and scintillator. Here energy loss and time-of-flight served to identify particles. Both detector systems cleanly separated tritons from all other reaction products, mainly deuterons.

The targets investigated are listed in table 1. The areal densities were determined from the energy loss of α-particles from an α-source or by elastically scattering 46 MeV ^{3}He ($\theta_L \geqq 9°$) and comparing with optical model calculations for the cross sections. The latter, however, were not purely Rutherford ($\sigma \lesssim 0.9\,\sigma_R$) so that some uncertainty is therefore introduced. We estimate that the ρx values listed in table 1 are accurate to $\pm 10\,\%$ for Sn and $\pm 15\,\%$ for Te.

TABLE 1
Targets

Nucleus	Enrichment [a]) (%)	ρx [b]) (μg/cm^2)	Nucleus	Enrichment [a]) (%)	ρx [b]) (μg/cm^2)
^{112}Sn	72.3	370	^{122}Sn	92.3	350
^{112}Sn	72.3	60	^{124}Sn	94.7	400
^{114}Sn	51.7	400	^{124}Te	91.9	50
^{116}Sn	95.7	240	^{125}Te	91.2	90
^{117}Sn	84.2	300	^{126}Te	98.7	32
^{118}Sn	96.6	570	^{128}Te	99.2	56
^{119}Sn	84.5	335	^{130}Te	99.5	47
^{120}Sn	98.4	290			

[a]) Supplied by Isotope Sales Division of Union Carbide Corporation, Oak Ridge National Laboratory, Oak Ridge, Tenn., USA.
[b]) Estimated error: Sn isotopes $\pm 10\,\%$; Te isotopes $\pm 15\,\%$.

The beam energy was determined using the momentum crossover technique [4]). Triton and deuteron groups arising from the reactions ^{40}Ca(^{3}He, t)^{40}Sc($E_x = 0.772$ MeV) and ^{37}Cl(^{3}He, d)^{38}Ar($E_x = 4.877$ MeV) were recorded in nuclear emulsions at $\theta_L = 0°$. With the Q-values taken from the compilation of Endt and Van der Leun [5]), the momenta of the two reaction products coincide at a bombarding energy $E_{^3\mathrm{He}} = 45.952 \pm 0.004$ MeV. The beam energy was determined to be 45.902 ± 0.010 MeV from the observed relative peak positions. The estimated uncertainty includes the stated uncertainties in the calibration Q-values [5]). Measurements of the beam energy on different occasions using this technique yielded values which were reproducible to within 5 keV.

With the beam energy fixed the ^{37}Cl(^{3}He, d)^{38}Ar reaction leading to states in ^{38}Ar at 2.168, 4.877, and 5.552 MeV was used to calibrate the spectrograph over the range of magnet excitation used in the (^{3}He, t) IAS measurements. The excitation energies of these states are all known [5]) to less than 1 keV. The relationship between optic-axis momentum and spectrograph field (as measured by a fixed NMR probe) was found to be linear within the uncertainty introduced in determing peak positions ($E/\Delta E \approx 20000$).

The energy resolution obtained with the PSD system was 20 to 30 keV (FWHM), depending on target thickness, which permitted peak centroid measurements to

better than ± 6 keV (± 1 mm). Most of the errors in determination of the triton energies arose from uncertainties in the beam energy and corrections for energy loss in the target (see subsect. 3.2).

The total beam current on target was deduced using a monitor detector which was calibrated before and after each 0° run with the Faraday cup in place.

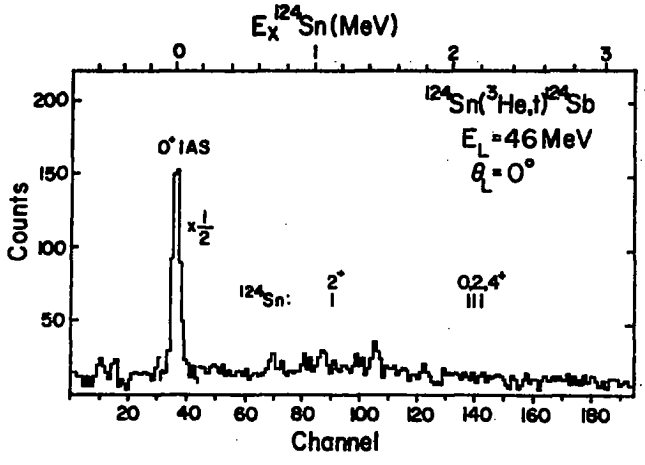

Fig. 2. A ^{124}Sn(^{3}He, t)^{124}Sb spectrum, obtained with a proportional counter, in the region of excitation in ^{124}Sb expected for the ^{124}Sn g.s. IAS. We indicate the calculated position (and energy) of ^{124}Sn excited IAS.

3. Data

3.1. SPECTRA

A position spectrum for the ^{124}Sn(^{3}He, t)^{124}Sb reaction at $\theta_L = 0°$ is shown in fig. 2. This was obtained with a proportional counter in the focal plane of AM1 and covers about 4 MeV excitation energy in ^{124}Sb including the expected position of the g.s. analog of ^{124}Sn. A single triton group, assumed to arise from that state, dominates the spectrum. We indicate in fig. 2 the positions expected for the 2^+ and 0^+, 2^+, 4^+ excited analog states of ^{124}Sn. At $\theta_L = 0°$ they are populated, if at all, several times more weakly than the 0^+ IAS. This result is not unexpected as $l = 0$ transitions are especially favored at $\theta_L = 0°$.

Spectra for $^{124,\ 125,130}$Te(^{3}He, t) to the g.s. IAS in ^{124,125,130}I are shown in fig. 3. They were obtained with a PSD in AM2 and each spectrum spans about 270 keV. We observe the following features for both the Sn and Te targets: The widths, Γ, of the IAS in general increase with increasing A for the even-A as well as the odd-A nuclei, but the widths in the odd-A nuclei are typically $1\frac{1}{2}$ to 2 times larger than those of the adjacent even-A nuclei. Also, the 0° cross sections increase with increasing target mass.

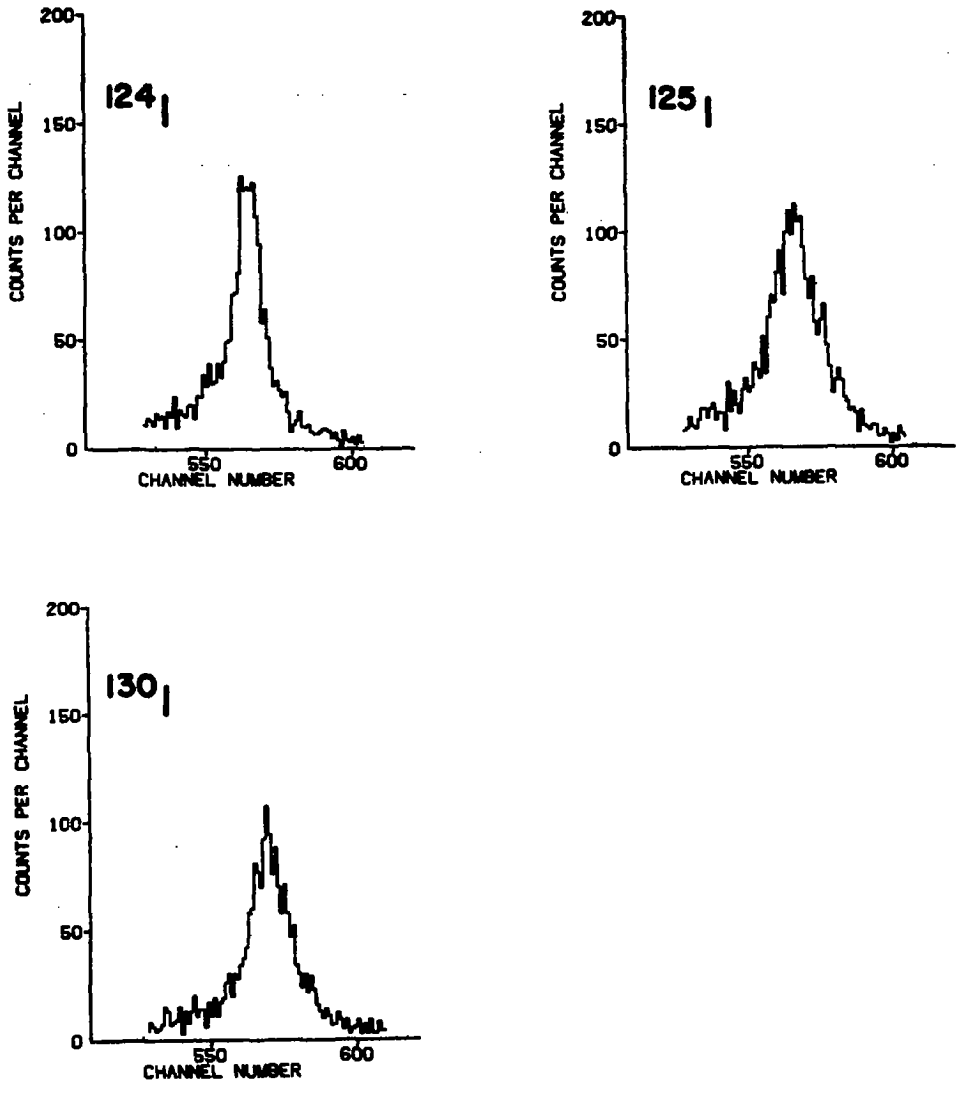

Fig. 3. Ground state IAS of ^{124,125,130}Te observed for Te(^{3}He, t)I at $\theta = 0°$. The data were obtained with a single solid-state PSD and span about 270 keV excitation energy.

The even-odd effect observed in the widths is not due to unresolved low-lying excited analogs of the odd-A targets. In ^{117}Sn and ^{124}Sn excited analogs, which should have been cleanly resolved, were searched for and observed to have $< 10\,\%$ of the strength of the g.s. $J^\pi = \frac{1}{2}^+$ or 0^+ IAS ($l = 0$).

TABLE 2
Coulomb displacement energies and IAS widths

Pair	A	J^π [a])	This work		Other work
			ΔE_C [b]) (keV)	Γ [c]) (keV)	ΔE_C [d]) (keV)
Sn-Sb	112	0^+	14019	26	13968 (50)[e])
	113	$\frac{1}{2}^+$			13948 (19)
	114	0^+	13940	10	13889 (50)[e])
	115	$\frac{1}{2}^+$			13896 (17)
	116	0^+	13861	34	13860 (20)
	117	$\frac{1}{2}^+$	13810	38	13804 (9)
	118	0^+	13789	26	13774 (8)
	119	$\frac{1}{2}^+$	13728	39	13740 (8)
		$\frac{3}{2}^+$			13738 (15)
	120	0^+	13729	32	13701 (7)
	121	$\frac{1}{2}^+$			13681 (14)
		$\frac{3}{2}^+$			13668 (11)
	122	0^+	13667	35	13644 (50)[e])
	123	$\frac{1}{2}^+$			13613 (12)
		$\frac{3}{2}^+$			13607 (12)
	124	0^+	13596	33	13561 (50)[e])
	125	$\frac{1}{2}^+$			13565 (16)
		$\frac{3}{2}^+$			13561 (13)
Te-I	123	$\frac{1}{2}^+$			14122 (20)
	124	0^+	14098	22	
	125	$\frac{1}{2}^+$	14065	49	14063 (14)
		$\frac{3}{2}^+$			14062 (14)
	126	0^+	14038	24	14061 (20)
	127	$\frac{1}{2}^+$			14010 (12)
		$\frac{3}{2}^+$			14005 (12)
	128	0^+	13985	22	
	129	$\frac{1}{2}^+$			13955 (14)
		$\frac{3}{2}^+$			13954 (14)
	130	0^+	13937	37	
	131	$\frac{1}{2}^+$			13910 (11)
		$\frac{3}{2}^+$			13900 (11)

[a]) Spin and parity of parent state [1-3]). The Coulomb energies are those for the lowest-lying states of the indicated J^π, which are not necessarily the parent ground state.

[b]) Absolute error, ± 20 keV; relative error, ± 10 keV (see text).

[c]) Total width of the indicated IAS assuming a Lorentzian line shape and corrected for the experimental resolution. Total error is ± 9 keV; relative error, ± 5 keV.

[d]) Unless otherwise noted, the ΔE_C values are from the compilation of W. J. Courtney and J. D. Fox, At. Data and Nucl. Data Tables 15 (1975) 141 adjusted slightly using recent neutron separation energies [7]). Errors are given in parentheses.

[e]) ΔE_C values from the proton decay energies of ref. [11]) and neutron separation energies of ref. [7]). Errors are given in parentheses.

3.2. COULOMB DISPLACEMENT ENERGIES

The Coulomb displacement energies for the Sn-Sb and Te-I g.s. IAS pairs have been deduced from the experimental (^{3}He, t) Q-values with

$$\Delta E_C = -Q(^3\mathrm{He}, \mathrm{t}) + \Delta, \tag{3.1}$$

where $\Delta = 764$ keV is the Coulomb displacement energy [6]) between ^{3}He and ^{3}H. The total uncertainty in the absolute ΔE_C values is estimated to be ± 20 keV. The relative ΔE_C values are accurate to ± 10 keV, however. Our data are presented in table 2, together with other results. The latter are mostly Coulomb energies deduced from energies presented in a recent tabulation combined with the latest neutron separation energies [7]). Overall, the different sets of Coulomb energies agree within quoted errors, although our values tend to be systematically larger, particularly when compared with the (p, n$\bar{\mathrm{p}}$) results. In this regard an independent, more direct measurement of the ^{40}Ca(^{3}He, t) Q-value, which was used as one of our main calibration points, would be useful.

The ΔE_C values (table 2) are observed to decrease less rapidly than the expected $A^{-\frac{1}{3}}$ dependence. This behavior can be seen more clearly by plotting $\Delta E_C - \Delta E_C^{\mathrm{calc}}$ where $\Delta E_C^{\mathrm{calc}}$ is calculated from a semi-empirical formula assuming a spherical charge distribution. We have used [8])

$$\Delta E_C^{\mathrm{calc}} = (1389 Z_< - 2041)/A^{\frac{1}{3}}\ \mathrm{keV}, \tag{3.2}$$

where $Z_<$ is the atomic number of the target. The difference $\Delta E_C - \Delta E_C^{\mathrm{calc}}$ is shown in fig. 4 for the Sn–Sb and Te-I data for the $J^\pi = \frac{1}{2}^+$ and 0^+ IAS. The maximum deviations from eq. (3.2) are about 80 keV in the extreme cases.

Odd-even variations in ΔE_C are generally small. The Coulomb energies for the odd-A Sn-Sb and Te-I $J^\pi = \frac{1}{2}^+$ pairs typically differ by less than 20 keV from neighboring

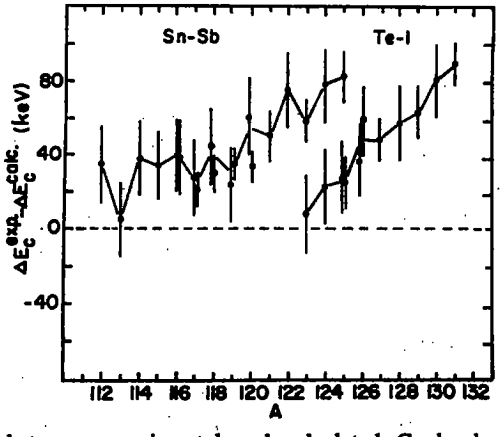

Fig. 4. Differences between experimental and calculated Coulomb displacement energies [eq. (3.2)]. Filled circles: this experiment; open circles: other experiments; $J^\pi = 0^+$ or $\frac{1}{2}^+$ (table 2). The solid lines connect values for adjacent isotopes and are only to guide the eye.

even-A, $J^\pi = 0^+$ pairs, although they do appear to be consistently lower (fig. 4). A similar situation applies to the $J^\pi = \frac{1}{2}^+$ pairs as the Coulomb energies for these nuclei are identical, within errors, to those for $J^\pi = \frac{1}{2}^+$ (table 2).

An interpretation of the Coulomb energy data is presented in sect. 4.

3.3. IAS WIDTHS

Total intrinsic widths, Γ, of the IAS have been deduced from the observed peak widths (see figs. 2 and 3) by unfolding the experimental line-widths arising from detector resolution, energy straggling in the target, etc. Uncertainties in this procedure limit the accuracy in Γ to ± 9 keV, where the lines are assumed to have a Lorentzian shape. Relative changes in Γ should be accurate to ± 5 keV, however. The total intrinsic widths Γ so obtained are listed in table 2 and compared in fig. 5 with other data, mostly from proton s-wave analog state resonances [1-3]). The three overlapping points $^{117, 119}$Sn-Sb and ^{125}Te-I agree within the assigned errors.

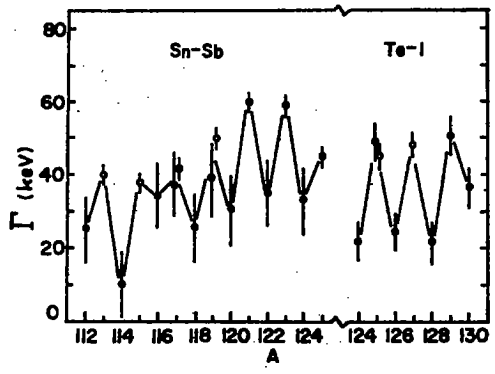

Fig. 5. Total width of IAS. Filled circles: this experiment; open circles: other experiments [1-3]). Even-A: $J^\pi = 0^+$; odd-A: $J^\pi = \frac{1}{2}^+$. The lines connect widths for adjacent isotopes and are only to guide the eye.

As seen in fig. 5 and in the raw data (fig. 3), there is a pronounced odd-A even-A variation of the Γ-values. The widths for the odd-A nuclei (s-wave resonances, $J^\pi = \frac{1}{2}^+$) are typically 10 to 30 keV larger than for adjacent even-A IAS. The widths for the even-A as well as the odd-A nuclei tend to increase with increasing A within the two isotopic sequences. The A-dependence of Γ is closely correlated with the excitation and binding energies of the IAS. This relation will be discussed in subsect. 4.2.

3.4. THE (^{3}He, t) CROSS SECTIONS

The (^{3}He, t) cross sections leading to the g.s. IAS measured at $\theta_L = 0°$ is shown in fig. 6 as a function of neutron excess. Also displayed are (p, n) and (p, n$\bar{\text{p}}$) total cross sections [9-11]). As expected the (^{3}He, t), (p, n) and (p, n$\bar{\text{p}}$) cross sections are closely related.

A simple charge-exchange mechanism between equivalent nucleons predicts [12]) a $(N-Z)/A^n$ variation of the (^{3}He, t) and (p, n) cross sections where $n \approx 2$. In fig. 6 we have included a curve with an $(N-Z)/A^2$ dependence, normalized to ^{118}Sn. The charge-exchange cross sections increase faster than $(N-Z)/A^2$ for $N-Z < 18$ and then remain constant for $N-Z \geqq 18$. The (^{3}He, t) data for Te are less accurate than those for Sn due to the increased peak widths (fig. 3) and other experimental uncertainties. (The Sn-Sb data are mostly the result of two or more independent measurements.)

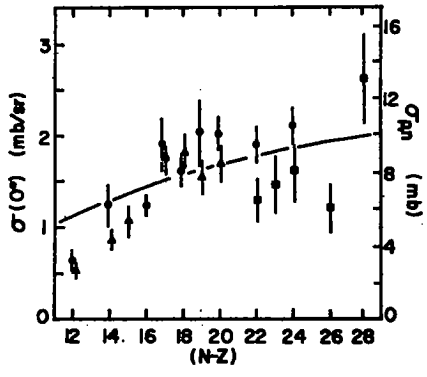

Fig. 6. The (^{3}He, t) cross sections at 0° (left scale) and (p, n) total cross sections (right scale). Filled circles and squares: (^{3}He, t) to g.s. IAS for Sn-Sb and Te-I isotopes (this work); open triangles: (p, n) or (p, n$\bar{\text{p}}$) measurements [9-11]). The curve represents an $(N-Z)/A^2$ dependence, arbitrarily normalized for ^{118}Sn.

The change in the dependence with $N-Z$ of the cross sections near $A \approx 118$ is possibly correlated with systematic changes occuring in the values of ΔE_C and Γ in this mass region (see figs. 4 and 5). This may indicate a shell effect and will be investigated below. It should be noted that in this mass region the (^{3}He, t) and (p, n) cross sections are *not*, as is often assumed in analysis of (p, n$\bar{\text{p}}$) data [10,11]), simple functions of $(N-Z)/A^2$.

4. Interpretation

4.1. COULOMB DISPLACEMENT ENERGIES

The following expression for the Coulomb displacement energies in heavy ($N \neq Z$) nuclei has been used [13-16]):

$$\Delta E_C = \Delta E_C^d + \Delta E_C^e + \Delta E_C^{s.o.} + \Delta E_C^{corr}. \tag{4.1}$$

Here ΔE_C^d is the direct term, ΔE_C^e is the exchange term, $\Delta E_C^{s.o.}$ is the electromagnetic spin-orbit energy, and ΔE_C^{corr} represents the remaining (small) corrections to ΔE_C.

The dominant, direct term is given by [13-15])

$$\Delta E_C^d = \frac{1}{2T}\int V_C(r)\rho_{exc}(r)d^3r, \tag{4.2}$$

where $V_C(r)$ is the target Coulomb potential and $\rho_{exc}(r)$ is the density distribution of the neutron excess. Expressions for the other terms can be found in the literature [15,16]) Application [14, 15]) of eqs. (4.1) and (4.2) to the experimental Coulomb energies for the Sn and Te isotopes yields information about the rms radii of $\rho_{exc}(r)$. The result, keeping only the first three terms of eq. (4.1), is

$$\langle r_{exc}^2\rangle^{\frac{1}{2}} - \langle r_p^2\rangle^{\frac{1}{2}} = 0.20 \pm 0.15 \text{ fm}, \tag{4.3}$$

where $\langle r_p^2\rangle^{\frac{1}{2}}$ is the measured rms radius of the proton point distributions [17]). Combining $\langle r_{exc}^2\rangle^{\frac{1}{2}}$ with the measured proton radii yields

$$\langle r_n^2\rangle^{\frac{1}{2}} - \langle r_p^2\rangle^{\frac{1}{2}} = 0.05 \pm 0.03 \text{ fm}, \tag{4.4}$$

for the difference between neutron and proton distributions rms radii. Here we assume that the proton and $N = Z$ core neutron distributions have the same rms radii. This is a crucial assumption and renders the result eq. (4.4) model dependent.

The uncertainties in eqs. (4.3) and (4.4) are large owing to unreliable estimates for the correction terms ΔE_C^{corr} appearing in eq. (4.1). Some of the problems in evaluating eq. (4.1) may be circumvented by considering instead the isotope shifts $\delta(\Delta E_C)$ in the Coulomb energies. Such a procedure also exploits the high relative accuracy of the measured values of ΔE_C (see table 2).

It is easy to show from eq. (4.1) that [15])

$$\frac{\delta(\Delta E_C^d)}{\Delta E_C^d} \approx -\frac{1}{2}\frac{\delta(\langle r_{exc}^2\rangle^{\frac{1}{2}})}{\langle r_{exc}^2\rangle^{\frac{1}{2}}} - \frac{1}{2}\frac{\delta(\langle r_p^2\rangle^{\frac{1}{2}})}{\langle r_p^2\rangle^{\frac{1}{2}}}.$$

If the isotope shifts in ΔE_C^s, $\Delta E_C^{s,o}$, etc. are ignored, one obtains

$$\frac{\delta(\langle r_{exc}^2\rangle^{\frac{1}{2}})}{\langle r_{exc}^2\rangle^{\frac{1}{2}}} \approx -\left[\frac{\delta\langle r_p^2\rangle^{\frac{1}{2}}}{\langle r_p^2\rangle^{\frac{1}{2}}} + 2\frac{\delta(\Delta E_C)}{\Delta E_C}\right], \tag{4.5}$$

where it is assumed that $\langle r_{exc}^2\rangle^{\frac{1}{2}} \approx \langle r_p^2\rangle^{\frac{1}{2}}$. More precise expressions are available [18]) if $\langle r_{exc}^2\rangle^{\frac{1}{2}} \neq \langle r_p^2\rangle^{\frac{1}{2}}$.

The isotope shift coefficient γ for a quantity X is usually defined by

$$\gamma \equiv \frac{3A}{X}\frac{\delta X}{\delta N},$$

where δN is the change in neutron number N. The quantity γ thus indicates the relative change in X with N. Specifically, it denotes the exponent in

$$X \propto A^{\frac{1}{3}\gamma}.$$

Thus $\gamma = \pm 1$ describes an $A^{\pm\frac{1}{3}}$ dependence of X. Eq. (4.5) implies that

$$\gamma_{exc} = -(\gamma_p + 2\gamma_{\Delta E_C}). \tag{4.6}$$

We present in fig. 7 the $\gamma_{\Delta E_C}$ values calculated from the isotope shift of the experimental ΔE_C values between the even-A pairs A-2 and A. Also presented in fig. 7 are the γ_p values measured for the proton distribution [17]. As indicated in fig. 7, the ΔE_C values decrease somewhat less than $A^{-\frac{1}{3}}$, i.e. $|\gamma|$ is less than unity for most pairs. The radii of the proton distribution however, increase at a rate much slower than $A^{\frac{1}{3}}$ (approximately $A^{\frac{1}{6}}$).

The variation in γ for $\langle r^2_{exc}\rangle^{\frac{1}{2}}$ deduced using eqs. (4.5) and (4.6) is shown in fig. 8. Here γ is > 1, i.e., as neutrons are added the rms radius of the neutron excess increases more rapidly than $A^{\frac{1}{3}}$. This result is in sharp contrast to the dependence on N of the rms radius of the proton distribution which increases much more slowly. Such effects are not unreasonable since N is increasing while Z remains constant. Limits on the variation with N of $\langle r^2_m\rangle^{\frac{1}{2}}$, the rms radius of the nuclear matter distribution can also be obtained as follows: Using values of $\delta\langle r^2_{exc}\rangle^{\frac{1}{2}}$ and $\delta\langle r^2_p\rangle^{\frac{1}{2}}$ (fig. 8), we assume that the rms radius of the $N = Z$ core neutrons changes no faster than $\langle r^2_{exc}\rangle^{\frac{1}{2}}$ and no slower than $\langle r^2_p\rangle^{\frac{1}{2}}$, i.e.,

$$\delta\langle r^2_p\rangle^{\frac{1}{2}} \leqq \delta\langle r^2_{n\,core}\rangle^{\frac{1}{2}} \leqq \delta\langle r^2_{exc}\rangle^{\frac{1}{2}}. \tag{4.7}$$

The isotope shifts, γ_p and γ_{exc} appropriately weighted by N and Z, can then be combined to yield the isotope shift γ_m of the rms radius of the nuclear matter distribution. Our results are shown in fig. 9, where the two curves represent the limits set by eq. (4.7). The analysis of ΔE_C values thus indicates that the radius of the nuclear matter distribution increases more slowly than $A^{\frac{1}{3}}$ for the Sn and Te isotopes, particularly if one assumes $\delta\langle r^2_{n\,core}\rangle^{\frac{1}{2}} \approx \delta\langle r^2_p\rangle^{\frac{1}{2}}$. The latter assumption is probably the most realistic one within the limits set by eq. (4.7). It therefore appears that the mass radius increase is *much* less than $A^{\frac{1}{3}}$ ($\approx A^{\frac{1}{6}}$). Similar effects have been observed in the Ca, Ti and Cr isotopes [19]. It is known, however, that nuclear saturation requires that, on the average, $\langle r^2_m\rangle^{\frac{1}{2}}$ increases as $A^{\frac{1}{3}}$. Based on the data shown in fig. 9, one would conclude that $\langle r^2_m\rangle^{\frac{1}{2}}$ must increase faster than $A^{\frac{1}{3}}$ in other mass regions. We have extended our (^{3}He, t) measurements to the deformed rare earth nuclei and preliminary results have been reported [20].

We have compared our results for $\delta(\langle r^2_{exc}\rangle^{\frac{1}{2}})$ and γ_{exc} with calculations made using a Woods-Saxon potential. The $N-Z$ excess neutrons were placed in $3s_{\frac{1}{2}}$, $2d_{\frac{3}{2}}$, $1h_{\frac{11}{2}}$, $2d_{\frac{5}{2}}$ and $1g_{\frac{7}{2}}$ orbitals with occupation probabilities given by BCS theory (see subsect. 4.3). Several extremes were considered: the potential radius, R_{WS}, was varied as $A^{\frac{1}{3}}$ ($\gamma_{WS} \approx 1$, curves (a) and (c)) or, alternatively, R_{WS} was kept constant ($\gamma_{WS} \approx 0$, curve (b)). The results are displayed in fig. 10 and compared with our "experimental" values of γ_{exc} for $\langle r^2_{exc}\rangle^{\frac{1}{2}}$. It can be seen that in both cases the calculated $\langle r^2_{exc}\rangle^{\frac{1}{2}}$ increase at a rate faster than the potential radius, i.e., $\gamma_{exc} > \gamma_{WS}$. The calculations with $R_{WS} \propto A^{\frac{1}{3}}(\gamma_{WS} \approx 1)$ qualitatively reproduce the experimental γ_{exc}, including the

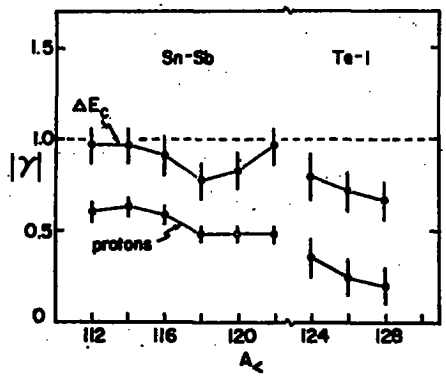

Fig. 7. Isotope shifts in Coulomb displacement energies (this work) and proton distribution rms radii [17]) relative to an $A^{\frac{1}{3}}$ dependence ($\gamma = 1$) between $A_< = A-2$ and $A_> = A$ (see text).

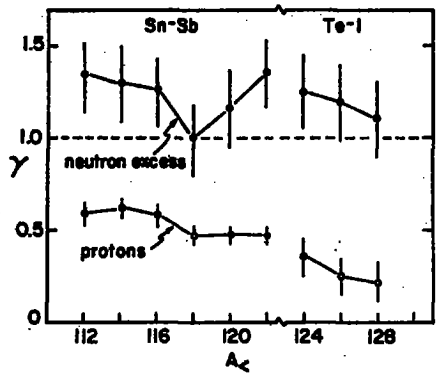

Fig. 8. Same as fig. 7 except shift in rms radius of neutron excess as deduced from Coulomb energies [eq. (4.5)] is shown.

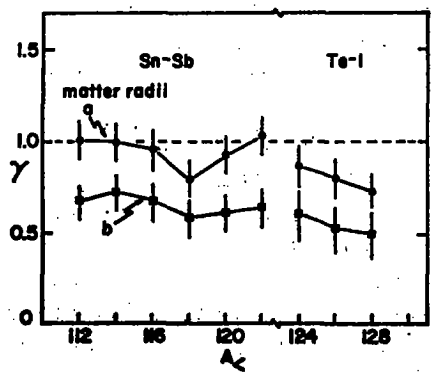

Fig. 9. Isotope shift γ_m of the matter radii deduced from shifts in Coulomb energies, and proton distribution (fig. 7). Curve (a): the neutron-core radius changes as the excess neutrons. Curve (b): the neutron-core radius varies as that of the proton distribution (see text).

decrease at $A = 118$. Better quantitative agreement would be obtained if R_{ws} increased slightly less than $A^{\frac{1}{3}}$, i.e., $\gamma_{ws} \approx 0.8$. The latter value is consistent with the variation of the matter radius, γ_m, deduced from our ΔE_C data (fig. 9).

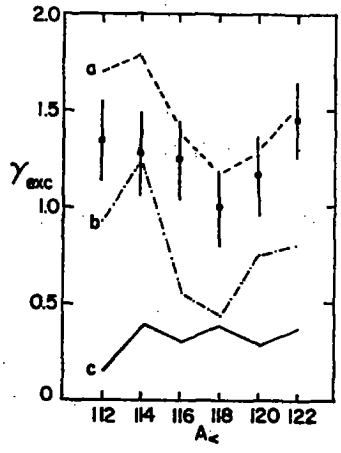

Fig. 10. Comparison of calculated and "experimental" isotope shifts γ_{exc} (see fig. 8) of the rms radius of the neutron excess in the Sn isotopes. The curves represent γ_{exc} calculated from BCS wave functions [28]) generated in a Woods-Saxon potential. Curve (a): $R_{ws} = 1.19A^{\frac{1}{3}}$ fm, ($\gamma_{ws} \approx 1$), V_{ws} was adjusted to fit the experimental neutron separation energies. Curve (b): R_{ws} = constant = 5.80 fm ($\gamma_{ws} \approx 0$), V_{ws} was adjusted to fit the experimental neutron separation energies. Curve (c): $R_{ws} = 1.19A^{\frac{1}{3}}$ fm ($\gamma_{ws} \approx 1$), V_{ws} = constant = 50.5 MeV, with the neutron separation energies varied. The other parameters are: $a_{ws} = 0.75$ fm, $V_{s.o.} = 5.5$ MeV, $R_{s.o.} = 1.01A^{\frac{1}{3}}$ fm, $a_{s.o.} = 0.75$ fm.

Thus, the Coulomb energy data and the calculations with the Woods-Saxon potential yield a self-consistent picture, namely, $1.5 \gtrsim \gamma_{exc} \gtrsim 1.0$, while $1.0 \gtrsim \gamma_m \gtrsim 0.5$ for the even-A tin isotopes.

The internal consistency of the results noted above appears to contradict recent suggestions [21]) that the Coulomb displacement energies are relatively independent of the neutron excess radii.

The analysis presented above concerns the data for the even-A nuclei. As noted in subsect. 3.2, however, there is a $\lesssim 20$ keV odd-even shift in ΔE_C for the Sn-Sb and Te-I isobaric pairs. Such a change in behavior in ΔE_C appears to be associated with the spins of the odd-A nuclei [15, 19]). The odd-A Sn nuclei and ^{125}Te have $J^{\pi}_{g.s.} = \frac{1}{2}^+$, i.e., the odd quasiparticle is in a $3s_{\frac{1}{2}}$ orbital while $^{127, 129, 131}$Te have $J^{\pi}_{g.s.} = \frac{3}{2}^+$, i.e., a $2d_{\frac{3}{2}}$ quasiparticle. There are several possible origins of the odd-even variation in ΔE_C [refs. [15, 16])]. There are, however, many effects each contributing 10 to 100 keV, with various signs, which can result in odd-even effects. As discussed elsewhere [15, 16]), most of these effects can only be estimated. At the moment, there is no single satisfactory explanation for the observed odd-even behavior of the Coulomb displacement energies [15, 16, 19]).

4.2. IAS WIDTHS

The total width, Γ, of an IAS can be written as the sum of T-allowed and T-forbidden partial decay widths [16, 22, 23]). We have used the following expression:

$$\Gamma = \Gamma_W + \sum_C \Gamma_C^{DR}, \tag{4.8}$$

where Γ_C^{DR} are the partial widths in the T-allowed decay channels (mostly proton and and γ decay) and Γ_W is the "spreading" width. The spreading width includes the compound nucleus widths and isospin-forbidden direct decay channels (e.g., neutron decay).

The spreading width, at least in the absence of external mixing is simply related to an average isospin mixing off-diagonal Coulomb matrix element $\langle V_{CD}^2 \rangle$ by [23])

$$\Gamma_W \approx 2\pi \langle V_{CD}^2 \rangle / D, \tag{4.9}$$

where D is the average spacing of $T_<$ states near the IAS having the same spin and parity as the IAS. We may determine $\langle V_{CD}^2 \rangle$ from the Sn-Sb data for $A < 116$ as neutron decay is energetically not allowed. Above $A = 116$ the neutron decay widths must be included, which along with D can be obtained from neutron resonance work [24]). If, in addition we assume that the proton decay widths are small (a few keV) for the even-A nuclei [10, 11]), we obtain experimental spreading widths Γ_W between 10 and 34 keV for the even-A tin isotopes. Using an average level spacing $D(J^\pi = 0^+)$ in Sb at $E_x \approx 9$ MeV of 220 eV/level as measured in neutron resonance work [24]), eq. (4.9) implies

$$\langle V_{CD}^2 \rangle^{\frac{1}{2}} \approx 0.6 - 1.1 \text{ keV}, \tag{4.10}$$

for the even-A Sb isotopes, $A \lesssim 116$. Due to uncertainties in determining $D(J^\pi = 0^+)$, our result [eq. (4.10)] is only an order-of-magnitude one, however it is comparable with values of $\langle V_{CD} \rangle$ as determined in this mass region in other measurements (0.5 to 4 keV) [25]).

The variation of Γ between adjacent odd-A and even-A nuclei and the increase of Γ with increasing A can be ascribed to the A-dependence of the single-particle partial widths Γ_p and Γ_α, respectively. These widths depend sensitively on the particle decay energies, which change with A. This correlation is illustrated in fig. 11 where we display the neutron and proton binding energies together with the excitation energy of the IAS in the Sb and I residual nuclei. Superimposed on the energy systematics is the variation of Γ, the IAS total width (fig. 6). It can be seen that Γ is related to E_x(IAS) and the proton-decay energy, E_p.

As the increase in Γ for odd-A nuclei appears to be associated mainly with E_p, at least for $J^\pi = \frac{1}{2}^+$ (fig. 11), we may use the difference in Γ between even-A and odd-A isotopes as a measure of Γ_p, the proton partial decay width. This procedure assumes that Γ for the even-A nuclei ($J^\pi = 0^+$) is dominated by the spreading width, Γ_W, and that Γ_W varies smoothly between isotopes and may be interpolated. As before,

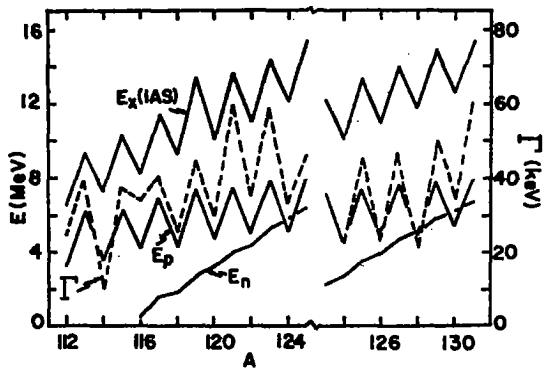

Fig. 11. The excitation (E_x), proton binding energy (E_p), and neutron binding energy (E_n) of IAS in Sn-Sb and Te-I [refs. [6,7])]. Superimposed on the energy systematics (solid lines) is the variation (fig. 5) of the total widths for $J^\pi = 0^+$ or $\frac{1}{2}^+$ IAS (dashed lines).

TABLE 3
IAS widths of odd-A nuclei

Nuclei	A	J^π	This work [a])			Other work [b])		
			Γ^p (keV)	$\Gamma-\Gamma^p$ (keV)	Γ^p/Γ	Γ^p (keV)	$\Gamma-\Gamma^p$ (keV)	Γ^p/Γ
Sn-Sb	113	$\frac{1}{2}^+$		17	0.61 [c])	10.3	30	0.26
	115	$\frac{1}{2}^+$		22	0.36 [c])	8	30	0.21
	117	$\frac{1}{2}^+$	8	30	0.21	16.5	26	0.39
	119	$\frac{1}{2}^+$	10	29	0.25	17	33	0.34
	121	$\frac{3}{2}^+$		32	0.23 [c])	7.5	32	0.18
		$\frac{1}{2}^+$		32	0.75 [c])	24	36	0.47
	123	$\frac{3}{2}^+$		34	0.21 [c])	7	35	0.19
		$\frac{1}{2}^+$		34	0.50 [c])	17	42	0.41
Te-I	125	$\frac{1}{2}^+$	26	23	0.53	12.2	33	0.27
	127	$\frac{3}{2}^+$		24	0.24 [c])	5.7	38	0.13
		$\frac{1}{2}^+$		24	0.57 [c])	13.7	35	0.28
	129	$\frac{3}{2}^+$		28	0.22 [c])	6.2	45	0.12
		$\frac{1}{2}^+$		28	0.35 [c])	9.9	38	0.21

[a]) Estimated error ±5 keV.
[b]) Refs. [1-3]). Errors are quoted as ±20 %.
[c]) Calculated using the Γ^p values from refs. [1-3]) and the $\Gamma-\Gamma^p$ values deduced from this work.

this assumption is valid if Γ_p for the even-A nuclei is small ($\lesssim 5$ keV), as is indeed indicated by (p, n$\bar{p}$) measurements [10, 11]).

The values of Γ_p and $\Gamma-\Gamma_p$ ($\approx \Gamma_W$) extracted in the manner outlined above are listed in table 3. We also calculate the ratio Γ_p/Γ and compare these with values determined from proton resonances [1-3]). Our values for $\Gamma-\Gamma_p$ tend to be smaller

than those determined from resonance work as is Γ_p for ^{117,119}Sn-Sb ($\frac{1}{2}^+$), while for ^{125}Te-I ($\frac{1}{2}^+$) our Γ_p is larger. This result may indicate some inadequacies in our interpolation procedure for $\Gamma - \Gamma_p$. As noted previously, however, our values for the total IAS widths Γ are in good agreement with (p, n$\bar{\text{p}}$) and proton resonance work.

4.3. CROSS SECTIONS AT 0°

Although the main motivation of the present experiment was not cross section measurements, the close relation to the (p, n) and (p, n$\bar{\text{p}}$) total cross sections (fig. 6) suggests that the 0° (^{3}He, t) data may be useful in extracting information on the effective $t \cdot t$ nuclear force. We have analyzed the 0° (^{3}He, t) data with a microscopic model [26, 27]).

The effective force between the target nucleons and the ^{3}He projectile was taken to be a Yukawa force with inverse range, μ, of 1 fm^{-1} (ms radius = 6 fm^2). The IAS wave functions were derived from semi-empirical BCS wave functions appropriate for the Sn isotopes [28]). The optical model parameters were extrapolated from the global set B1 of ref. [29]).

The average strength (and mean deviation) of the effective force required to fit our data for even-A ($J^\pi = 0^+$) isotopes is

$$V_{t \cdot t} = 11 \pm 4 \text{ MeV}, \tag{4.11}$$

for $\mu = 1$ fm^{-1} (we use the same definition of effective force as in refs. [30, 31])). This strength corresponds to a volume integral of 138 ± 50 MeV · fm^3 for the effective $t \cdot t$ force.

Our result [eq. (4.11)] is to be compared with the values $V_{t \cdot t} \approx 40$–60 MeV ($\mu = 1$ fm^{-1}) deduced from analyses [30, 31]) of ^{90}Zr(^{3}He, t) for $E_{^3\text{He}} \approx 30$ to 70 MeV. The values of $V_{t \cdot t}$ deduced from (^{3}He, t) measurements, especially at $\theta = 0°$, are sensitive ($\approx$ factor of two) to the optical model parameters as both the ^{3}He and triton are strongly absorbed. The triton parameters, particularly, are highly uncertain as they are extrapolated well beyond the energy region of existing triton elastic scattering data. Nevertheless our value of $V_{t \cdot t}$ is smaller than the values obtained from study of the (^{3}He, t) and (p, n) reactions on lighter nuclei [12, 26, 29–31]).

It has recently been noted [32]) that some (^{3}He, t) reactions apparently proceed by the two-step process (^{3}He, α) (α, t). Even through such processes are most important for anti-analog and non-analog states some contributions to transitions to g.s. IAS are also predicted [32]). Although we have made no estimates of the two-step contributions to our data or the other relevant data [30, 31]), these may be large enough to modify our conclusions regarding the relative magnitudes of the effective force deduced from the various analyses of the (^{3}He, t) reaction.

One feature observed in the microscopic calculation is the large variation in (^{3}He, t) cross sections for different orbitals. The cross section for charge exchange of an $1h_{\frac{11}{2}}$ neutron is twice that of $2d_{\frac{5}{2}}$ or $1g_{\frac{7}{2}}$ and five times that of $3s_{\frac{1}{2}}$. The $1h_{\frac{11}{2}}$ orbital, it should be noted, is an "intruder" level from the next major oscillator shell and thus

has a larger radial extent (rms radius) than the other orbitals. Although our particular calculations do not reproduce the observed variation in cross sections for the even-A isotopes (fig. 6), this is mostly due to uncertainty in the isotopic variation of the optical potentials. It is clear, however, that shell effects can easily account for the isotopic variations observed in the (^{3}He, t) cross sections, and one cannot *a priori* assume a simple dependence on neutron excess within an isotopic sequence.

5. Conclusions

We conclude the following from the study of IAS in the Sn and Te isotopes using the (^{3}He, t) reaction at 0°:

(i) The Coulomb displacement energies decrease less rapidly than an $A^{-\frac{1}{3}}$ dependence. This result when combined with the known isotopic variation of the radius of the proton distribution ($\approx A^{\frac{1}{3}}$) implies that the neutron-excess radius increases slightly faster than $A^{\frac{1}{3}}$ and the total nuclear matter radius of Sn and Te increases less than $A^{\frac{1}{3}}$, perhaps substantially less.

(ii) The total IAS widths exhibit a marked odd-A even-A effect. This behavior can be understood in terms of a variation of the single-particle decay widths, primarily the proton decay width, with decay energy. The data yield proton widths and spreading widths. The latter correspond to an isospin-violating matrix element of about 1 keV.

(iii) The 0° (^{3}He, t) cross sections are related to (p, n) total cross sections and may be used to obtain information on the $t \cdot t$ effective force. The Sn and Te data, however, indicate an effective force about one-fourth that obtained in previous analyses for lighter nuclei, assuming a simple direct charge exchange.

We thank the cyclotron crew and staff for their assistance. We also thank D. Robson and G. T. Garvey for information concerning interpretation of the IAS widths.

References

1) P. Richard, C. F. Moore, J. A. Becker and J. D. Fox, Phys. Rev. **145** (1966) 971
2) D. D. Long, P. Richard, C. F. Moore and J. D. Fox, Phys. Rev. **149** (1966) 906
3) J. L. Foster, Jr., P. J. Riley and C. F. Moore, Phys. Rev. **175** (1968) 1498
4) D. R. Back *et al.*, Rev. Sci. Instr. **27** (1956) 516;
G. F. Trentleman and E. Kashy, Nucl. Instr. **82** (1972) 304
5) P. M. Endt and C. van der Leun, Nucl. Phys. **A214** (1973) 1
6) A. H. Wapstra and N. B. Gove, Nucl. Data Tables **9** (1971) 267
7) A. Wapstra and K. Bos, At. Data and Nucl. Data Tables, **17** (1976) 474
8) J. Jänecke, Isospin in nuclear physics, ed. D. H. Wilkinson (North-Holland, Amsterdam, 1969) ch. 8
9) J. D. Carlson, Ph. D. thesis, University of Colorado, 1972 (unpublished);
J. D. Carlson, C. D. Zafiratos and D. A. Lind, Nucl. Phys. **A249** (1975) 29
10) P. S. Miller and G. T. Garvey, Nucl. Phys. **A163** (1971) 65
11) C. A. Whitten, Jr., J. Chai, N. Chirapatpimol, W. H. Dunlop and G. Igo, Phys. Lett. **51B** (1974) 45

12) V. A. Madsen, Nuclear isospin, ed. J. D. Anderson *et al.* (Academic Press, New York, 1969) p. 149
13) J. A. Nolen, Jr. and J. P. Schiffer, Phys. Lett. **29B** (1969) 396;
J. P. Schiffer, J. A. Nolen, Jr. and N. Williams, Phys. Lett. **29B** (1969) 399
14) E. Friedman and B. Mandelbaum, Nucl. Phys. **A135** (1969) 472
15) J. A. Nolen and J. P. Schiffer, Ann. Rev. Nucl. Sci. **19** (1969) 471
16) N. Auerbach, J. Hüfner, A. K. Kerman and C. M. Shakin, Rev. Mod. Phys. **44** (1972) 48
17) J. R. Ficenec, L. A. Fajardo, W. P. Trower and I. Sick, Phys. Lett. **42B** (1972) 213, and references cited therein;
A. F. Mezentsev *et al.*, Yad. Fiz. **11** (1970) 1141 [Engl. transl.: Sov. J. Nucl. Phys. **11** (1970) 633]
18) J. Jänecke, Nucl. Phys. **A181** (1972) 49
19) F. D. Becchetti, D. Dehnhard and T. G. Dzubay, Nucl. Phys. **A168** (1971) 151
20) J. Jänecke, R. Tickle, W. S. Gray, E. Sugarbaker and F. D. Becchetti, Bull. Am. Phys. Soc. **19** (1974) 995
21) N. Auerbach, Nucl. Phys. **A229** (1974) 447
22) D. Robson, Phys. Rev. **137** (1965) B535;
D. Robson, Isospin in nuclear physics, ed. D. H. Wilkinson (North-Holland, Amsterdam, 1969) ch. 10;
D. Robson, private communication
23) A. M. Lane, Isopin in nuclear physics, ed. D. H. Wilkinson (North-Holland, Amsterdam, 1969) ch. 11;
A. Z. Mekjian, Nucl. Phys. **A146** (1970) 288;
H. A. Weidenmüller, Nucl. Phys. **A99** (1967) 289
24) A. Gilbert and A. G. W. Cameron, Can. J. Phys. **43** (1965) 1446;
U. Facchini and E. Saetta, Energia Nucleare **15** (1968) 54
25) R. J. Blin-Stoyle, Isospin in nuclear physics, ed. F. H. Wilkinson (North-Holland, Amsterdam, 1969) ch. 4
26) G. R. Satchler, Isospin in nuclear physics, ed. D. H. Wilkinson (North-Holland, Amsterdam, 1969) ch. 9
27) V. A. Madsen, Nucl. Phys. **80** (1966) 177;
G. R. Satchler, Nucl. Phys. **77** (1966) 481; **A95** (1967) 1
28) E. Schneid, A. A. Prakash and B. L. Cohen, Phys. Rev. **156** (1967) 1316;
D. G. Fleming, M. Blann, H. W. Fulbright and J. A. Robbins, Nucl. Phys. **A157** (1970) 1, and references cited therein
29) F. D. Becchetti, W. Makofske and G. W. Greenlees, Nucl. Phys. **A190** (1972) 437
30) W. L. Fadner, J. J. Kraushaar and S. I. Hayakawa, Phys. Rev. **C5** (1972) 859
31) R. A. Hinrichs and D. L. Show, Phys. Rev. **C6** (1972) 1257
32) L. D. Rickersten *et al.*, Phys. Lett. **60B** (1975) 19, and references cited therein